A Generalization of Using an Adjoint Model in Intermittent Data Assimilation Systems

XIANG-YU HUANG

Danish Meteorological Institute, Copenhagen, Denmark

(Manuscript received 21 August 1997, in final form 10 May 1998)

ABSTRACT

A generalized setup is proposed for the poor man's 4D variational data assimilation system (PMV) of Huang et al. The new scheme is referred to as a generalization of PMV (GPV) and has the same basic idea as that of PMV, that is, to use an adjoint model to improve an optimum interpolation (OI)–based assimilation system. In addition, GPV includes the possibility of using different forecast models in the original OI-based assimilation system and in the variational component of the scheme. This generalization leads to three advantages over the original setup: 1) a wider application of an adjoint model developed for a particular forecast model; 2) an implementation flexibility due to its incremental nature; 3) considerable CPU savings when the variational component is run on low resolutions.

A detailed comparison is made between GPV and PMV. The steps of a practical implementation are also given. A 5-day period characterized by intense cyclone development is chosen for testing different data assimilation schemes. Experiments with GPV using a low-resolution variational component based on different model formulations indicate that the proposed scheme GPV, as its predecessor PMV, also leads to better first guess fields, smaller analysis increments, modified baroclinic structures in the final analyses, and improved forecasts. The differences between the GPV analyses and the original OI-based analyses are mainly in the data-sparse area and are related to baroclinic processes.

1. Introduction

The idea of four-dimensional variational data assimilation (4DVAR) has been pursued for more than a decade from theoretical foundations to operational attempts (Le Dimet and Talagrand 1986; Lewis and Derber 1985; Derber 1987; Thépaut and Courtier 1991; Navon et al. 1992; Županski 1993; Thépaut et al. 1993). One of the remaining problems for an operational implementation of 4DVAR is its excessive demand for computer power due to the iterative nature of the minimization procedure used. Research efforts have been devoted to improving the minimization algorithm (Yang et al. 1996; Županski 1996; Wang et al. 1997) or using an incremental approach (Courtier et al. 1994). Schemes using only one 4DVAR minimization iteration together with an optimal interpolation (OI) scheme or with a three-dimensional variational data assimilation (3DVAR) have also been proposed for operational implementations on current computers (Huang et al. 1997; Pu et al. 1997b; Pu et al. 1997a).

The one-iteration approach is based on the idea that an analysis at a later time into the forecast could be used to improve the current forecast, as first proposed by Rabier et al. (1996). The forecast errors are calculated as the difference between a short-range forecast and the corresponding ''future'' analysis. The errors are traced back to the initial time by integrating the adjoint model. This integration yields a sensitivity field. Adding a portion of the sensitivity field to the initial state, the nonlinear forward model is integrated to produce a new forecast—the sensitivity forecast. Using a global model and its adjoint together with future analyses (48 h into the forecasts), Rabier et al. (1996) have shown that sensitivity forecasts are indeed better than the original forecasts, especially in the fast baroclinic development situations. Gustafsson and Huang (1996) have demonstrated that this idea also works in a limited-area model with analyses 6 h into the forecasts. The sensitivity forecasts are not real forecasts as they use future analyses. To extend this idea one step further and use it in a preoperational environment, Huang et al. (1997) tried to include a variational component, the adjoint model, into an OI-based intermittent data assimilation system and referred to the scheme as a ''poor man's 4DVAR'' (PMV). The PMV scheme consists of 1) 6-h forward forecast model run, 2) preliminary OI analysis, 3) 6-h adjoint model backward run, 4) 6-h forward forecast run (sensitivity forecast), and 5) final OI analysis. Parallel experiments were conducted and the results indicated that the PMV analysis increments are smaller than the original OI increments; that the upper-air baroclinic

Corresponding author address: Danish Meteorological Institute, Lyngbyvej 100, DK-2100 Copenhagen Ø, Denmark.
E-mail: xyh@dmi.dk

structures have been improved by running the adjoint model backward in time and then the forecast model forward in time; and that based on observation verification, the overall performance of the PMV system is better than the original OI system. Pu et al. (1997b) and Pu et al. (1997a) proposed a very similar scheme using the 3DVAR scheme developed by Derber et al. (1991) and Parrish and Derber (1992). They investigated different methods for computing the sensitivity fields and a number of implementation configurations. Their results also point to consistent forecast quality improvements, especially in the Southern Hemisphere.

An operational implementation of PMV is technically a straightforward matter. However, at least two practical issues need to be addressed before a real parallel preoperational test can start.

1) The PMV scheme of Huang et al. (1997) (also that of Pu et al. 1997b; Pu et al. 1997a) requires additional CPU power and disk storage, although much less than for a full-sized 4DVAR. Most weather centers have selected an operational setup (e.g., data window, horizontal/vertical model resolutions, integration domain size) that uses the full capacity of their computer to meet the forecast delivery deadline. As discussed in Huang et al. (1997), the CPU requirement of using the PMV scheme is approximately that of doubling the horizontal resolution of the original OI system. In other words, we need to reduce the resolution of the current operational system in order to be able to run PMV. This reduction applies to both analysis and forecast. As in most adjoint model formulations, the basic-state variables at every forward time step are stored. The disk or central memory storage needed for running PMV is therefore significant. *The first question we would like to ask ourselves is, Could it be possible to run the adjoint model on a coarser resolution than that of the analysis and forecast model?*

2) The PMV scheme requires that the adjoint model should be developed from the same forecast model used by the original OI-based system. This may lead to practical difficulties. For example, the adjoint model used in Huang et al. (1997) is developed in the international High Resolution Limited Area Modelling project (HIRLAM). The HIRLAM forecasting system has been used operationally in many HIRLAM member countries with minor differences in each implementation. Although the adjoint model is based upon the spectral formulation of the HIRLAM forecast model, all current operational implementations use the gridpoint forecast model. This means that the forecast model in the data assimilation system needs to be replaced by the spectral model in order to run the PMV scheme. *The second question we would like to ask ourselves is, Could it be possible to use an adjoint of a forecast model that is different to that used in the OI-based (or 3DVAR-based) data assimilation system?* More specifically, can we use the adjoint of the spectral HIRLAM model together with the current operational data assimilation systems that have the gridpoint HIRLAM model as the forecast model?

The answers to the above questions also have theoretical implications. As in the two studies by Gustafsson and Huang (1996) and Huang et al. (1997), the model and selected synoptic weather situation are the same but the horizontal resolutions of the model are different. The results seem to indicate that the improvements due to backward adjoint calculation exist in both low- (Gustafsson and Huang 1996) and high-resolution (Huang et al. 1997) model setups. The PMV improvements should be due to an improved assimilation of significant dynamic and physical structures. The numerical formulation, for example, spectral or gridpoint representation, should influence the results less significantly.

In this study, we will make a generalization of PMV (GPV) that computes the modified first guess (steps 3–4 in PMV) incrementally. The GPV scheme adds only an increment to the preliminary first guess. Such an increment can be calculated on a different resolution with different model formulations. With the GPV scheme, we intend to provide answers to the two practical questions raised above. The GPV scheme is described in section 2, using the PMV as a reference. The experiment setups used in this study are given in section 3. The results from GPV on different resolutions and with spectral or gridpoint models are shown in section 4 and section 5 together with discussions. Concluding remarks are summarized in section 6.

2. The data assimilation schemes

Three data assimilation schemes are described below: 1) the OI-based data assimilation system OIA; 2) PMV of Huang et al. (1997); 3) the proposed GPV scheme. It is convenient to first define the following acronyms for the components of the schemes and their counterparts used in this study:

- ana—the OI/3DVAR scheme (in this study, the HIRLAM OI scheme);
- fom—the nonlinear forecast model used in the original OI/3DVAR-based data assimilation system (in this study, the HIRLAM spectral or gridpoint model);
- vfm—the nonlinear forecast model used in the adjoint model development, where v stands for variational (in this study, the spectral HIRLAM model); and
- adm—the adjoint of vfm (in this study, the adjoint of the spectral HIRLAM model).

In Fig. 1, OIA, PMV, and GPV are schematically summarized. The common component of all three schemes is the observation state *O*, which is formed by collecting observations (e.g., ± 3 h) around the analysis time (e.g., 0 h).

In the OIA scheme, ana and fom are needed. There are basically two steps.

OIA step 1—Forecast step (including initialization):

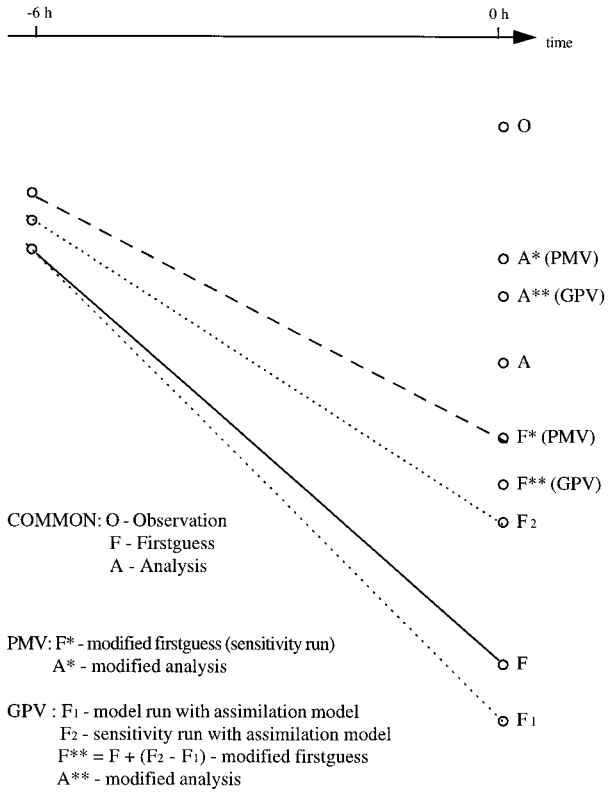

FIG. 1. Schematic representation of OIA, PMV, and GPV.

From the analysis in the previous data assimilation cycle (e.g., −6 h), a forecast is made by fom to produce a first guess *F* (the end of the slanted full line).

OIA step 2—Analysis step: Combining *F* with the observation state *O*, ana is performed to produce the analysis state *A* for the current data assimilation cycle.

In the PMV scheme, fom and vfm are identical and the resolution remains the same throughout the scheme. The adjoint model adm is needed in addition to ana and fom. As mentioned in the introduction, there are five steps in this scheme.

PMV step 1—The same as in the OIA forecast step except with an additional task, that is, to store the model state trajectory (the slanted full line) during the integration.

PMV step 2—The same as in the OIA analysis step.

PMV step 3—Adjoint step: Starting from the difference between the first guess and analysis, $F - A$, and using the stored model state trajectory as basic state, the adjoint model adm is integrated backward in time. The result of this step is the sensitivity field.

PMV step 4—Sensitivity forecast step: Adding a portion of the sensitivity field to the analysis at −6 h, the forecast model fom is run again to produce the modified first guess *F** (the end of the dashed line).

PMV step 5—Final analysis step: Combining the modified first guess *F** with the observation state *O*, ana is performed again to produce the final analysis *A**.

In the PMV scheme, steps 1 and 3 are coupled through the basic state and that is why fom and vfm should be identical.

In the GPV scheme fom and vfm could be different. Transforms between the two model formulations and/or their resolutions are needed. There are seven steps in this scheme.

GPV step 1—The same as the OIA forecast step.

GPV step 2—The same as in the OIA analysis step.

GPV step 3—Auxiliary forecast step: From the analysis at −6 h, an auxiliary forecast is made using vfm to produce a 6-h forecast F_1. During the integration, store the model state trajectory (the lower dotted line). The model state trajectory may be based on a different formulation (e.g., spectral in this step against grid point in steps 1, 2, and 7) and/or on a different resolution (e.g., low in this step against high in steps 1, 2, and 7).

GPV step 4—Adjoint step: Starting from the difference between the first guess and analysis, $F_1 - A$, and using the stored model state trajectory as basic state, the adjoint model adm is integrated backward in time. In this step, the preliminary analysis *A* needs to be transformed to the same format as F_1 (e.g., transformed from grid point to spectral formulation and/or interpolated from high to low resolution). The result of this step is the sensitivity field.

GPV step 5—Sensitivity forecast step: Adding a portion of the sensitivity field to the analysis at −6 h, the forecast model vfm is run again to produce the sensitivity forecast F_2 (the end of the upper dotted line).

GPV step 6—First guess modification step: The difference between the auxiliary forecast and the sensitivity forecast, after being transformed back to the same formulation and resolution as *F*, is added to the first guess *F* to form the modified first guess: $F^{**} = F + (F_2 - F_1)$.

GPV step 7—Final analysis step: Combining the modified first guess *F*** with the observation state *O*, ana is performed again to produce the final analysis *A***.

In the GPV scheme, steps 1 and 2 are exactly the same as those in the OIA scheme. The variational component in GPV, steps 3–6, can be completely separated from the rest of the scheme. From a practical point of view, the adjoint of the spectral HIRLAM model could be used in a data assimilation system that has the gridpoint HIRLAM model as the forecast model (or other OI/

3DVAR-based data assimilation system). The variational component could run on a lower resolution, demanding less CPU time and disk storage. Naturally, the generalization may also lead to problems due to the use of different model formulations and the interpolations between resolutions. The limitations of GPV will be further discussed in the next section, where the experiment setups are described.

To summarize, the GPV scheme is a generalization of PMV. The main advantages of GPV over PMV are the implementation flexibility and the possible CPU savings. If vfm is chosen to be fom and run on the same resolution as fom, GPV steps 3 and 6 become unnecessary and GPV reduces to PMV.

In appendix A, the GPV scheme in a formula form is described. In the formula form, the transforms between different grids and different resolutions are explicitly defined. The relations between GPV, PMV, and OIA are also given.

3. The experiment setups

A 5-day period, from 0000 UTC 13 September 1994 to 0000 UTC 18 September 1994, is chosen for the data assimilation experiments. The same period was also chosen for the sensitivity study by Gustafsson and Huang (1996) and the PMV study by Huang et al. (1997). The DMI analyses of the mean sea level pressure for this period are given in Fig. 2. In the beginning of the period, 0000 UTC 13 September 1994, a small low pressure system was over the Atlantic Ocean southwest of Ireland. This system developed into a major cyclone that hit Denmark and southern Sweden 3 days later and then significantly weakened at the end of the 5-day period. The baroclinic development of the cyclone was the dominant weather process in this period. It is shown in Gustafsson and Huang (1996) and Huang et al. (1997) that the sensitivity forecast leads to improvements in cases where baroclinic structures are not well handled by the OI analysis. This 5-day period is therefore a good choice for testing the GPV scheme. It should be noted that a 5-day period is too short to draw conclusions on the operational feasibility of the proposed method. Preoperational tests of GPV are planned for longer periods, two weeks in winter and two weeks in summer and the results will be reported separately.

To compare the performance of different data assimilation schemes, a +36-h forecast is launched from each analysis (21 forecasts in the 5-day period for each experiment). The forecasts are verified directly against observations from European rediosonde and synoptic stations to give an objective evaluation of the forecast quality. The forecasts are also compared with analyses from different data assimilation experiments. The operational Danish Meteorological Institute (DMI) observation verification package and field verification package are used. Twelve parameters are chosen as in the DMI operational setup: geopotential height Z; temperature T; wind vector **V** at 250 hPa, 500 hPa, and 850 hPa; mean sea level pressure (MSLP); 2-m temperature (T02M); and 10-m wind (V10M).

The HIRLAM data assimilation system is used to test the proposed GPV scheme. The system is developed in a collaborative research project among national meteorological institutes of Denmark, Finland, France, Iceland, Ireland, the Netherlands, Norway, Spain, and Sweden (Machenhauer 1988; Gustafsson 1993). It is an intermittent data assimilation system including an OI scheme and a forecast model. The system is documented in Källén (1996). A short description of the OI scheme is given in appendix B. The gridpoint forecast model is briefly described in Huang et al. (1994). The spectral HIRLAM and its adjoint model are described in Gustafsson (1991) and Gustafsson and Huang (1996).

The data flow of the HIRLAM data assimilation system is shown in Fig. 3 with the variational component in the large box excluded. Before the analysis time, the forecast model (fom) has produced the operational (+36 or +48 h) forecast that includes the first guess field to the coming data assimilation cycle (here FGS00). It needs to be stressed here that the forecast model could be either the spectral HIRLAM model or the gridpoint HIRLAM model. At the analysis time (e.g., $t = 0$), based on the first guess field (FGS00, a 6-h forecast) and the observations collected in the data window from −3 h to +3 h (OBS00), the OI scheme (ana) gives the analysis field (ANA00).

The proposed GPV scheme is also shown in Fig. 3 with the large box containing the variational component of GPV. As can be seen from the figure, this scheme is a flexible one—the variational component could be added in or removed from the data assimilation system at any time. The purpose of GPV is to modify the preliminary first guess FGS00 by adding an increment. This modification could be based on a different forecast model (here the spectral HIRLAM model) and its adjoint (Gustafsson and Huang 1996). After analysis and before forecast, the spectral HIRLAM (vfm) is run from the analysis in the previous cycle ANA18 to produce a model trajectory and a forecast VFG00, which can be on the original or a low resolution. Using the ANA00 as the ''truth'' (or ''observation'') and VFG00 as a ''guess,'' and using the model trajectory as basic state, the adjoint spectral model (adm) is integrated backward in time to produce a gradient field GRD18. Adding a portion of GRD18 to ANA18, the spectral HIRLAM model is run again to produce the sensitivity forecast VGF00*. The difference between the two spectral HIRLAM forecasts, VGF00 − VGF00*, which contains some information on the most unstable forecast error mode (Gustafsson and Huang 1996; Huang et al. 1997), is then added to the original first guess FGS00 to produce the modified first guess FGS00*. With OBS00 and FGS00*, the OI scheme is performed for the second time to yield the final analysis ANA00*.

In this paper, five experiments are presented. A sum-

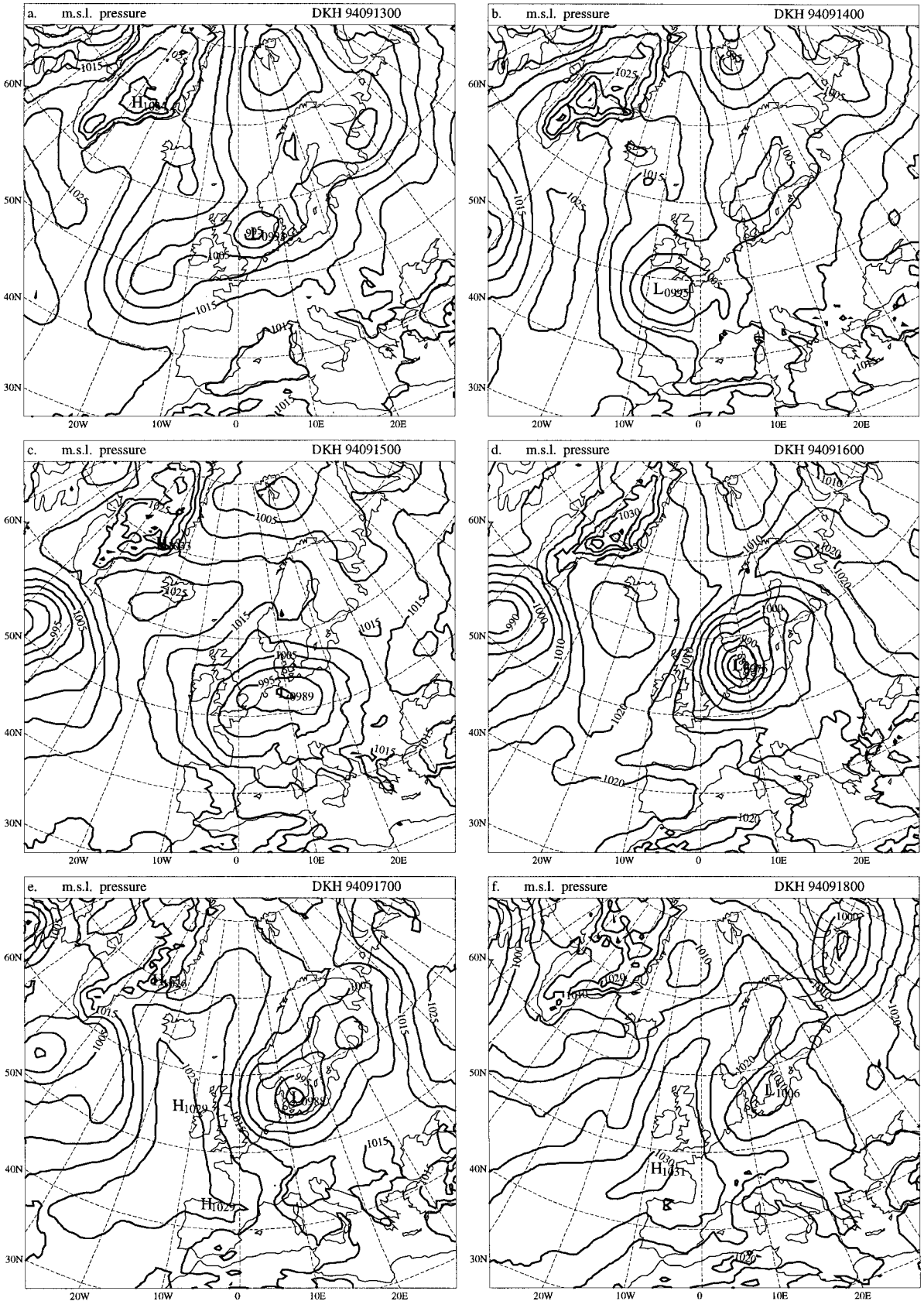

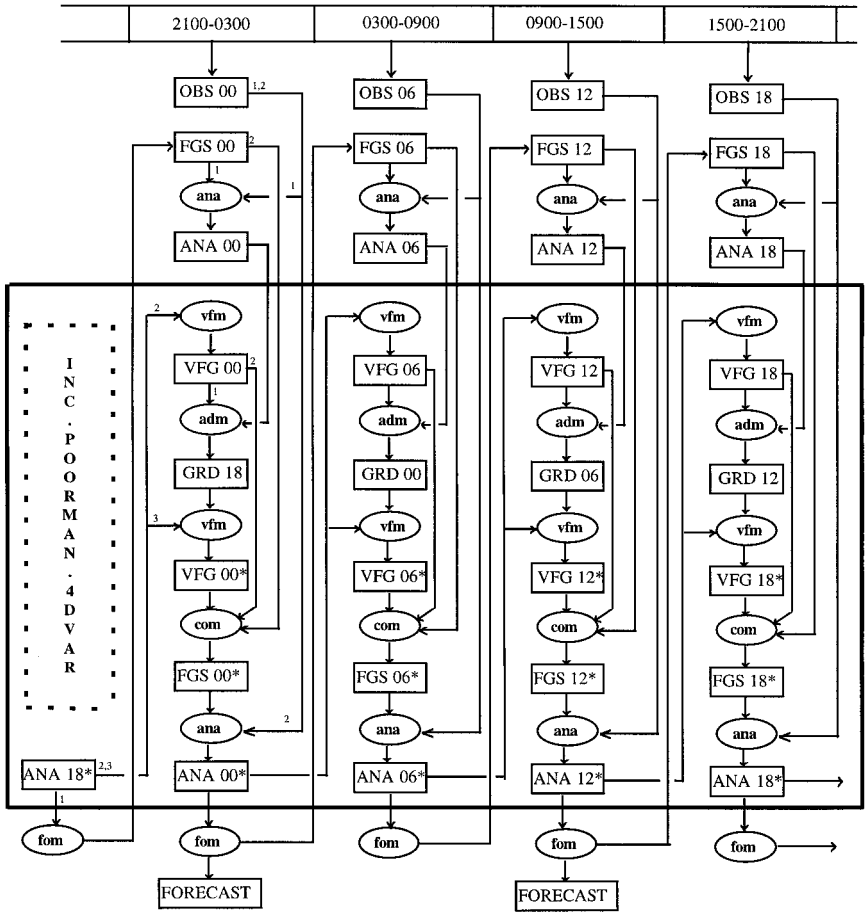

FIG. 3. Data flow for the HIRLAM operational data assimilation system (without the component in the large box) and for the GPV (with the large box). The small boxes are for fields and the number in the boxes is for time (00 for 0000 UTC, 06 for 0600 UTC, etc): OBS00, observation field; FGS00, preliminary first guess field; ANA00, preliminary analysis field; VFG00, auxiliary 6-h forecast field; GRD18, gradient field valid at −6 h (here 1800 UTC); VFG00*, 6-h sensitivity forecast field; FGS00*, modified first guess field; ANA00*, final analysis field; FORECAST, operational +36 h or +48 h forecast. The ellipses are for programs: ana, OI analysis; vfm, the forecast model used in the variational component; adm, the adjoint model; com, calculation of the modified firstguess; fom, the basic forecast model used in the original OIA scheme. The small numbers outside of a box indicate how many times the field is used.

mary is given in Table 1. The experiments are divided into two groups. In SOI, SSH, and SSL, the spectral HIRLAM model is used both in the original OI system and in the variational component. They are designed for testing the GPV algorithm and the resolution effect. In GOI and GSL, the gridpoint HIRLAM model is used in the original OI system and the spectral HIRLAM model is used in the variational component. They are designed for testing the influence of the mixed use of gridpoint formulation and spectral representation. In this group, an operational environment is used for both experiments. The GSL setup is suitable for further parallel testing and even for an operational implementation. Detailed descriptions of all experiments are given below.

SOI—This experiment uses the DMI operational data assimilation system with two modifications. 1) The forecast model in SOI is the spectral HIRLAM model. 2) The DMI analyses are used as lateral boundaries to reduce the effect of old boundaries. [In an operational environment, only delayed forecasts obtained from European Centre for Medium-

←

FIG. 2. Operational DMI HIRLAM analyses at (a) 0000 UTC 13 Sep 1994, (b) 0000 UTC 14 Sep 1994, (c) 0000 UTC 15 Sep 1994, (d) 0000 UTC 16 Sep 1994, (e) 0000 UTC 17 Sep 1994, (f) 0000 UTC 18 Sep 1994. The contour interval is 5 hPa.

TABLE 1. Summary of data assimilation experiments.

Experiment	Scheme	Grid	Modification	Lateral boundaries
SOI	OIA	Spectral	No	HIRLAM analyses
SSH	PMV*	Spectral	Full	HIRLAM analyses
SSL	GPV	Spectral	Incremental	HIRLAM analyses
GOI	OIA	Grid point	No	ECMWF forecasts
GSL	GPV	Mixed	Incremental	ECMWF forecasts

* In the SSH experiment, the scheme actually used is GPV. However, GPV is reduced to PMV due to the choice of the forecast model and resolution in this experiment.

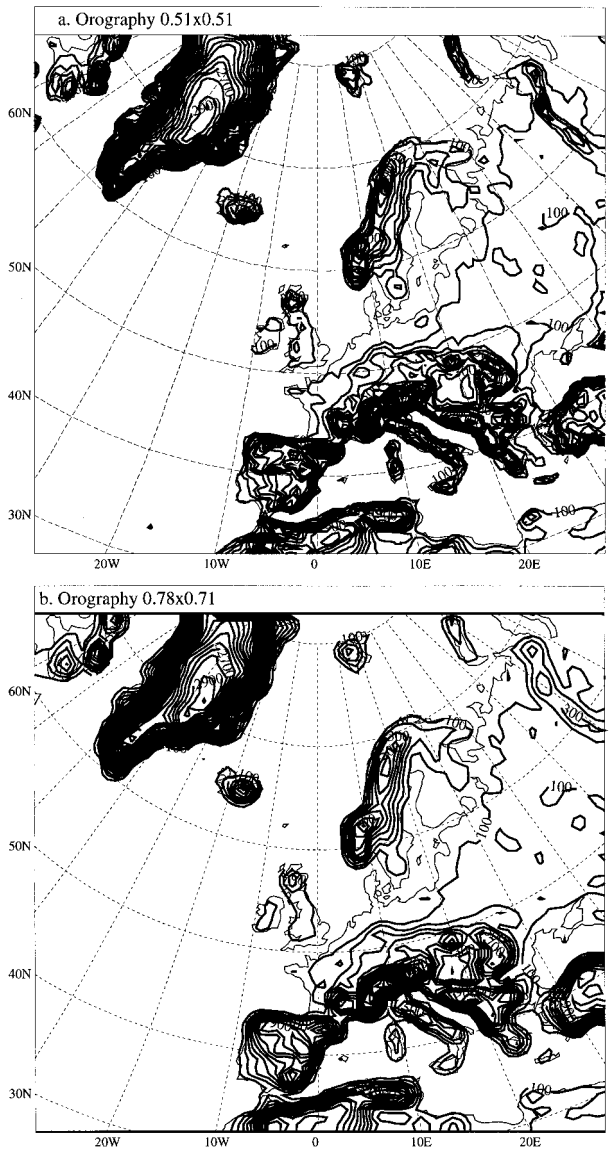

FIG. 4. The model domain and orography on (a) high and (b) low resolutions. The contour interval is 100 m and starts from 100 m.

Range Weather Forecasts (ECMWF) are available.] The transform grid resolution is 0.51°, corresponding to a shortest resolved wave of approximately 160 km, and is referred to as high resolution in this paper.

SSH—This experiment uses the proposed GPV scheme. The original OI part is the same as SOI, using the spectral HIRLAM model and analyzed boundaries. In the variational component, the model resolution is chosen to be the same as that for the OI analysis and forecast (the original OI part). As discussed in section 2, the GPV scheme reduces to the PMV scheme in this experiment because vfm and fom are the same and they are with the same resolution. This experiment is used to check the GPV algorithm: it should reproduce the PMV results of Huang et al. (1997). It is also used as a reference when experiments with reduced model resolution are performed.

SSL—This experiment uses the proposed GPV scheme. The setup differs from SSH only in the resolution used by the variational component. About two-thirds of the original horizontal resolution is used. This resolution (shortest resolved wave of approximately 240 km) is referred to as a low resolution in this paper. This experiment is designed for testing the effect of using low-resolution variational component.

GOI—This experiment uses the DMI operational data assimilation system without any change. The basic forecast model is the gridpoint HIRLAM model. The ECMWF forecasts available at the analysis time are used as lateral boundaries. This experiment is used as a reference for the next experiment.

GSL—This experiment uses the proposed GPV scheme. The original OI part is the same as GOI. In the variational component, the low resolution is chosen. This experiment is designed for testing the possibility of using a *low-resolution spectral* variational component in a gridpoint OI-based system. The setup could be used directly in preoperational parallel tests and even for an operational implementation.

The orography fields used by high and low resolutions are given in Figs. 4a and 4b, respectively. All interpolations between these two horizontal resolutions need

to be followed by an adjustment procedure, which modifies the interpolated fields according to the orography on the new resolution. As mentioned in section 2, the incremental nature of GPV could lead to problems. One possible problem source is due to this interpolation. In PMV, there is no such interpolation and the final analysis is based on a 6-h sensitivity forecast, which should be in a dynamical balance. In GPV, however, an increment $F_2 - F_1$ is added to the original balanced first guess. The dynamical balance is nonlinear, and therefore the difference between two 6-h forecasts may not be fully balanced. In addition, the interpolation introduces some noise depending on the difference between the two resolutions. Experiments with different low resolutions, down to 1.5° (not shown), indicated that the noise level in the final analysis is higher when the difference between the two resolutions becomes larger. The low resolution used in SSL and GSL appears to be a good choice from the noise level point of view.

When using mixed model formulations one needs to be especially cautious when going back and forth between the two formulations. For instance, the Arakawa C grid is used in the gridpoint HIRLAM model while the Arakawa A grid is used in the spectral HIRLAM model. The A-grid is nonstaggered while the C-grid is fully staggered (Arakawa and Lamb 1977). To avoid grid inconsistency, transforms are required between the A grid and C grid. The following simple transforms are used in GSL:

from C grid to A grid:

$$u^A_{1,j} = u^C_{1,j} \qquad j = 1, \text{jmax}$$

$$u^A_{i,j} = (u^C_{i-1,j} + u^C_{i,j})/2, \qquad i = 2, \text{imax}; \quad j = 1, \text{jmax}$$

$$v^A_{i,1} = v^C_{i,1}, \qquad i = 1, \text{imax}$$

$$v^A_{i,j} = (v^C_{i,j-1} + v^C_{i,j})/2, \qquad i = 1, \text{imax}; \quad j = 2, \text{jmax}$$

from A grid to C grid:

$$u^C_{1,j} = u^A_{1,j}, \qquad j = 1, \text{jmax}$$

$$u^C_{i,j} = 2 \cdot u^A_{i,j} - u^C_{i-1,j}, \qquad i = 2, \text{imax}; \quad j = 1, \text{jmax}$$

$$v^C_{i,1} = v^A_{i,1}, \qquad i = 1, \text{imax}$$

$$v^C_{i,j} = 2 \cdot v^A_{i,j} - v^C_{i,j-1}, \qquad i = 1, \text{imax}; \quad j = 2, \text{jmax},$$

where u and v are horizontal wind components in eastward and northward directions, superscripts A and C indicate A grid and C grid, subscripts i and j are gridpoint indices, and imax and jmax are the numbers of horizontal grid points in eastward and northward directions.

The following energy-related quadratic cost function J is used in this study:

$$J = \frac{1}{2} \sum_z \sum_y \sum_p \times \left[(\Delta u)^2 + (\Delta v)^2 + R_d T_r (\Delta \ln p_s)^2 + \frac{C_p}{T_r} (\Delta T)^2 \right],$$

where the summation is taken over all the horizontal and vertical grid points; the differences are calculated between analyzed and first guess winds (Δu and Δv), logarithms of surface pressure ($\Delta \ln p_s$), and temperature (ΔT); R_d is the gas constant for dry air; C_p is the specific heat at constant pressure for dry air; and T_r (=300 K) is a reference temperature. The gradient of J at the analysis time ($t = 0$ h) is projected back to the previous cycle ($t = -6$ h) by the adjoint model. The result is the sensitivity field

$$\nabla J_{t=-6} = \text{adm } \nabla J_{t=0}.$$

Adding a portion (α) of the sensitivity to the analysis at $t = -6$ h, the sensitivity run produces an improved first guess.

The final technical remark is given on α. This factor is related to the length of the backward/forward integration (Rabier et al. 1996; Gustafsson and Huang 1996). With a model resolution like the low resolution in this study, Gustafsson and Huang (1996) used 0.01 for 48-h, 0.03 for 12-h, and 0.1–0.5 for 6-h integration periods. With a model resolution like the high resolution in this study, Huang et al. (1997) used 0.2 in their PMV experiment. A large α normally gives rise to a large impact on the sensitivity forecast, bringing it closer to analysis. However, if α is too large, the sensitivity forecast could move farther away from the analysis than the original forecast. When experiments with different model formulations and resolutions are compared, it seems difficult to fix an α value. An objective choice of α is used in this study, using the method proposed by Derber (1987). Denote the energy-related inner product as $\langle , \rangle$ (the cost function defined early can then be rewritten as $J = \langle F - A, F - A \rangle$). The optimal α is estimated by assuming the forecast solutions vary linearly in the search direction, where the linear change is based on the difference between the current solution, F, and a solution produced from an initial field incremented in the search direction by α_g, F^g. The optimal α is given by

$$\alpha = \alpha_g \frac{\langle F - A, F - F^g \rangle}{\langle F - F^g, F - F^g \rangle},$$

where F^g is a +6-h forecast from the initial state $[A + \alpha_g \nabla J]_{t=-6}$, and α_g is the guess factor, which is 0.2 in this study.

4. Effect of using different resolutions

In the first group of experiments, vfm is the same as fom, that is, only the spectral HIRLAM model is used both in the original OI system and in the variational component. The effect of using different resolutions in the variational component is the main motivation for these experiments.

The 36-h forecasts from experiments SOI, SSH, and SSL for the rapid cyclone development between 1200 UTC 14 September and 0000 UTC 16 September are

compared first to demonstrate the impact of GPV on the forecast.

Using the SOI forecast as a reference, the differences in the surface pressure are plotted for SSH (Fig. 5) and SSL (Fig. 6), respectively. The evolution of the difference patterns in Fig. 5 is the same as that obtained by using the PMV scheme (Huang et al. 1997). This is expected because the GPV scheme should reduce to the PMV scheme when vfm is the same as fom and the same resolution is used for both the forward models and the adjoint model. One can notice that the significant difference patterns in Fig. 5 are related to the developing cyclone in Fig. 2. Using a low-resolution variational component, similar difference patterns are produced by SSL (Fig. 6). Although the amplitude of difference is somewhat changed, comparing Figs. 5 and 6, the patterns and locations remain almost the same in the forecasts. Decreasing the resolution even further from 0.75° (in SSL), the clear dipole pattern in Figs. 5 and 6 becomes much weaker (with resolution 1.0°) or even disappears (resolution 1.5°).

The bias and rms errors in the mean sea level pressure forecast are shown in Fig. 7 as functions of forecast length for this case (a single 36-h forecast in each experiment). It is evident that both SSH and SSL forecasts are better than the SOI forecast for this field. The major improvements occur after +18 h. The difference between SSH and SSL scores is small. It is interesting to note that the SSL forecast is comparable to SSH throughout the 36-h forecast period and even becomes better than SSH.

Averaged over the 5-day period (in total 21 forecasts), mean sea level pressure verification scores (Fig. 8j) remain similar to those from the case study (Fig. 7), although the forecast improvement is less dramatic. This is to be expected as the GPV scheme gives only forecast quality improvements in cases where upper-air structures are not well handled by the OI analysis scheme.

Other variables (e.g., wind and temperature) and other analyses/forecasts have been examined. The results are summarized by the observation verifications in Fig. 8. Both SSH and SSL forecasts are consistently better than the SOI forecasts in mean sea level pressure, geopotential height of all selected levels, temperature, and wind at high levels (250 hPa and 500 hPa). Only looking at the 36-h forecasts, SSH and SSL have better scores in almost all parameters. The low-level (850 hPa, 10 m, 2 m) wind and temperature verifications show little or no improvement using the proposed scheme. The SSH scores in Fig. 8 once again confirm the correctness of the GPV algorithm, compared with those of PMV in Huang et al. (1997). The SSL scores in Fig. 8 show that with a low-resolution variational component (less disk storage and CPU requirement than PMV) the GPV scheme can produce the same forecast improvement as for PMV.

Finally, the analysis increments for the preliminary analysis and for the final analysis over the 5-day period are shown in Figs. 9 and 10 for SSH and SSL, respectively. The analysis increments are significantly reduced in the final OI analyses. The low-resolution variational component gives the same qualitative impact, that is, produces modified first guess fields that are closer to observations than the preliminary first guess fields. A more detailed comparison reveals that the reduction of the analysis increments in SSL is not as large as that in SSH, especially in the high-level winds. However, this difference between SSH and SSL analysis increments seems to have no significant impact on the forecast results.

To summarize the results in this section, the following points may be stated.

- Compare the SSH results (in this section) to the PMV results in Huang et al. (1997), it is obvious that the GPV algorithm is correct.
- The low-resolution GPV (SSL) gives qualitatively similar results to that from high-resolution (SSH). It gives, for example, (i) modification in forecast flow patterns, (ii) improvement in forecast scores, and (iii) reduction in analysis increments. This answers the first question raised in the introduction: the variational component in the GPV data assimilation system can be run on a low resolution, giving rise to the considerable CPU usage and disk storage savings.
- The best choice of low resolution seems to be two-thirds of the original resolution. As shown in this section, SSL gives almost the same improvements over the original OI scheme as the SSH with only about $(\frac{2}{3})^3 \approx \frac{1}{3}$ CPU usage and disk storage [$(\frac{2}{3})^2$ in horizontal directions and $\frac{2}{3}$ in time].

Further reduction in resolution leads to degradation in results for the selected 5-day period (results not shown). In a recent study, a similar choice of low resolution has also been used in running incremental 4DVAR experiments based on subjective inspections of model error spectra.

5. Effect of using different model formulations

In the second group of experiments, the effect of using different model formulations is investigated. Although the original OI-based system uses the gridpoint HIRLAM forecast model, the variational component of GPV

→

FIG. 5. Difference in surface pressure between SSH and SOI forecasts at (a) +06 h, (b) +12 h, (c) +18 h, (d) +24 h, (e) +30 h, (f) +36 h. The forecasts are started from 1200 UTC 14 Sep 1994. The contour interval is 1 hPa. Full line is positive. Dashed line is negative. Zero line is suppressed.

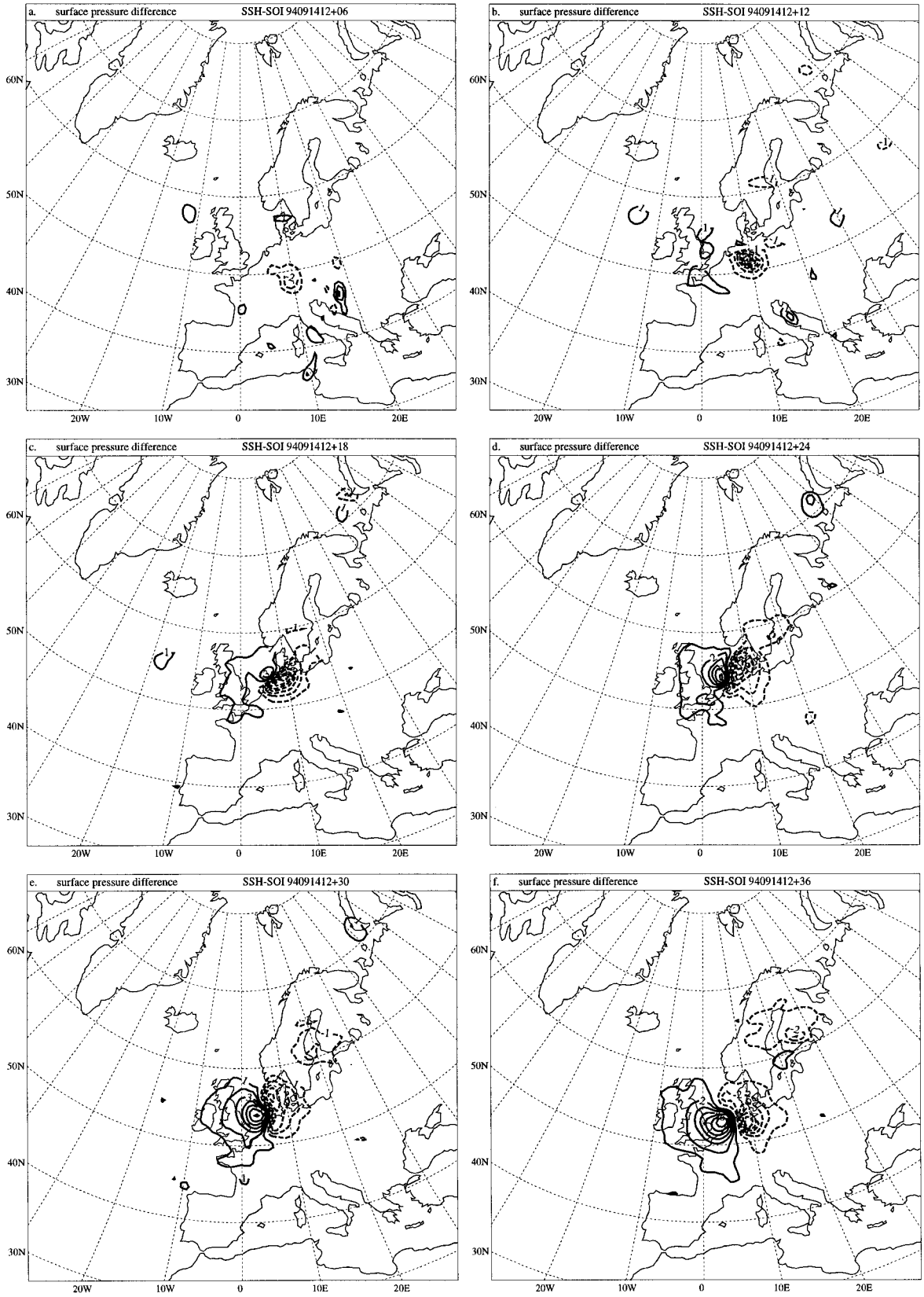

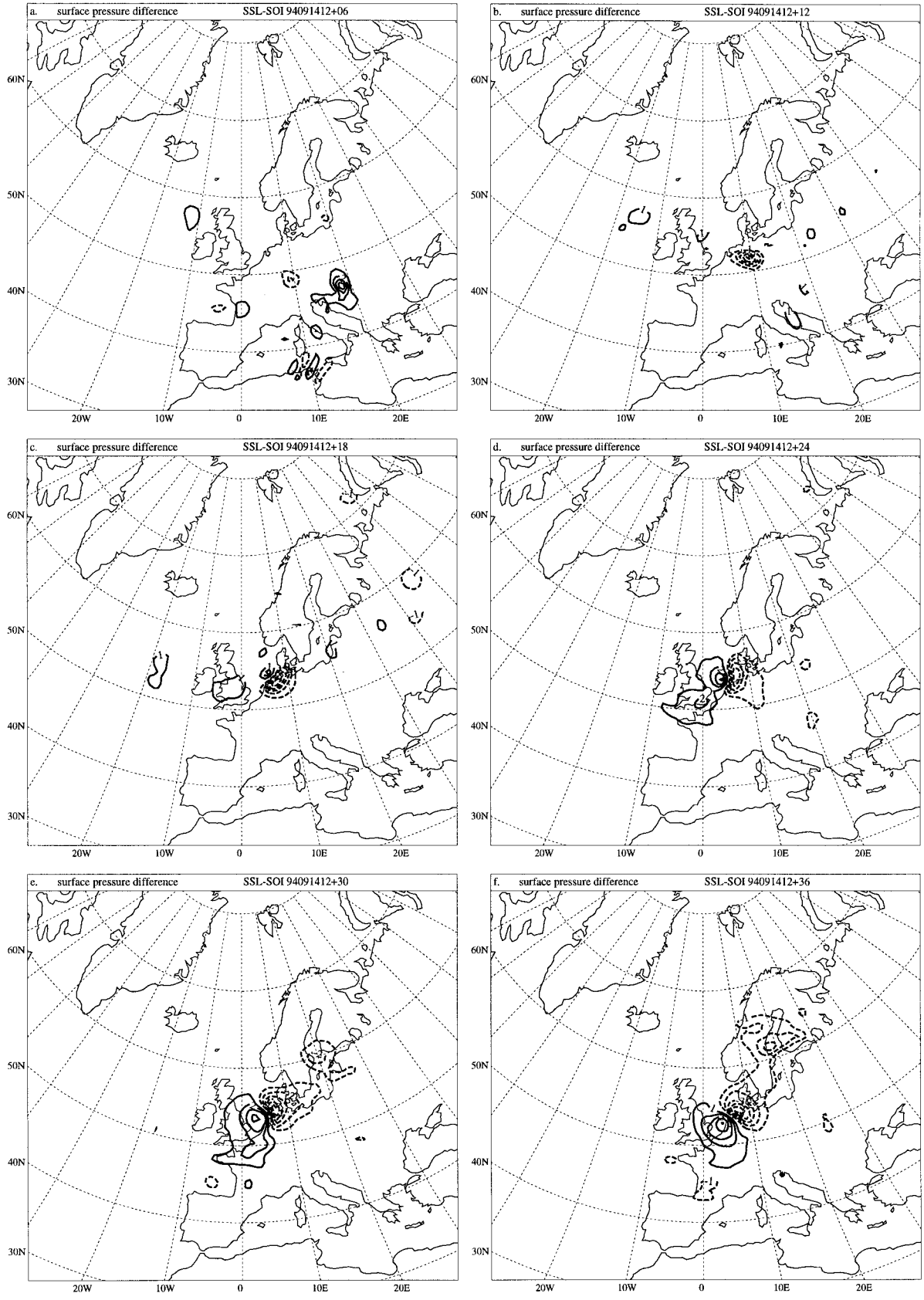

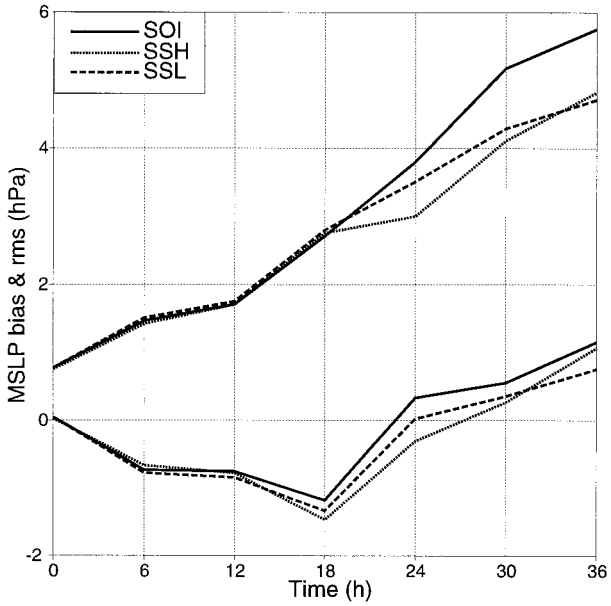

FIG. 7. Observation verification, bias (lower group of curves), and rms (upper group of curves) of mean sea level pressure (MSLP) as functions of forecast length for SOI (full lines), SSH (dashed lines), and SSL (dotted lines) for the 36-h forecasts starting from 1200 UTC 14 Sep 1994.

uses the spectral HIRLAM forecast model. In addition, with an operational implementation in mind, the variational component is also run on a low resolution (two-thirds of the original).

The natural way to proceed is to first look at the evolution of the forecast difference between GOI and GSL for the same case as in the previous section. It turns out, however, that the GPV improvements on the forecast for the development case in the previous section are insignificant because the original OI forecast is much better than that from SOI. In fact, the original OI forecast in the GOI experiment looks similar to those made in SSH and SSL. There seems to be very little space left for improvements by GPV. On the other hand, forecasts initiated from some other cycles (e.g., 0000 UTC 14 September, 1200 UTC 15 September) reveal similar difference patterns between GSL and GOI forecasts to those in Figs. 5 and 6. Thus different individual forecasts are improved by the GPV techniques depending on the different forecast model setups. Instead of showing these different individual forecasts, the observation verification scores for GOI and GSL over the 5-day period (21 forecasts) are given in Fig. 11. Both bias (lower two curves in each panel) and rms (upper two curves in each panel) are shown as functions of forecast length.

From Fig. 11, GSL forecasts are better than GOI forecasts in mean sea level pressure, geopotential height at all levels, temperature at 500 hPa and 2 m, wind at 500 hPa and 850 hPa. It is somewhat unexpected that the GSL forecasts for temperature and wind at 250 hPa become slightly worse than the GOI forecasts, a result opposite to that from the previous section. The reason behind this is still not clear. At the end of 36-h forecasts, GSL seems to have improvements in almost all selected parameters.

In GSL, there are two transforms, which are related to the variationally computed first guess increment $F_2 - F_1$: 1) between low and high resolutions, 2) between A and C grids. Low-level fields like 2-m temperature and/or 10-m wind are very sensitive to small errors in these transforms. The results in Fig. 11 at least indicate no obvious problem in these transforms.

So far only the observation verification package is used. The advantage of this package is its independence of any data assimilation system. Only a gross quality check is employed, which uses an analysis to reject observations with very large discrepancies. The disadvantage of the package is its coverage. Only the European radiosonde and synoptic observations are used. For the model geometry selected in this study, the verification covers only part of the model domain. A possible operational implementation of GPV at DMI would require a much larger domain. In that case, the observation verification package gives forecast scores for a very small portion of the model domain.

A field verification, which compares forecasts against verifying analyses, has no coverage problem. To give another view on the forecast quality and to keep an operational implementation in mind, we also show the field verification results for GOI and GSL. The DMI operational field verification package is used. The same parameters as those used in observation verification are chosen. The field verification package requires verifying analyses. In the comparison between GOI and GSL, there are two sets of analyses, one from each experiment. The analyses from different experiments could be quite different. For instance, the variational component in GSL is able to make changes in analyses over the ocean where no observation is available. To demonstrate the difference between the two analyses, the 5-day mean geopotential height analyses at 250 hPa, 500 hPa, and 850 hPa from GOI and GSL are given in Fig. 12 and the differences between GOI and GSL analyses, measured as bias and standard deviation, are given in Fig.

←

FIG. 6. Difference in surface pressure between SSL and SOI forecasts at (a) +06 h, (b) +12 h, (c) +18 h, (d) +24 h, (e) +30 h, (f) +36 h. The forecasts are started from 1200 UTC 14 Sep 1994. The contour interval is 1 hPa. Full line is positive. Dashed line is negative. Zero line is suppressed.

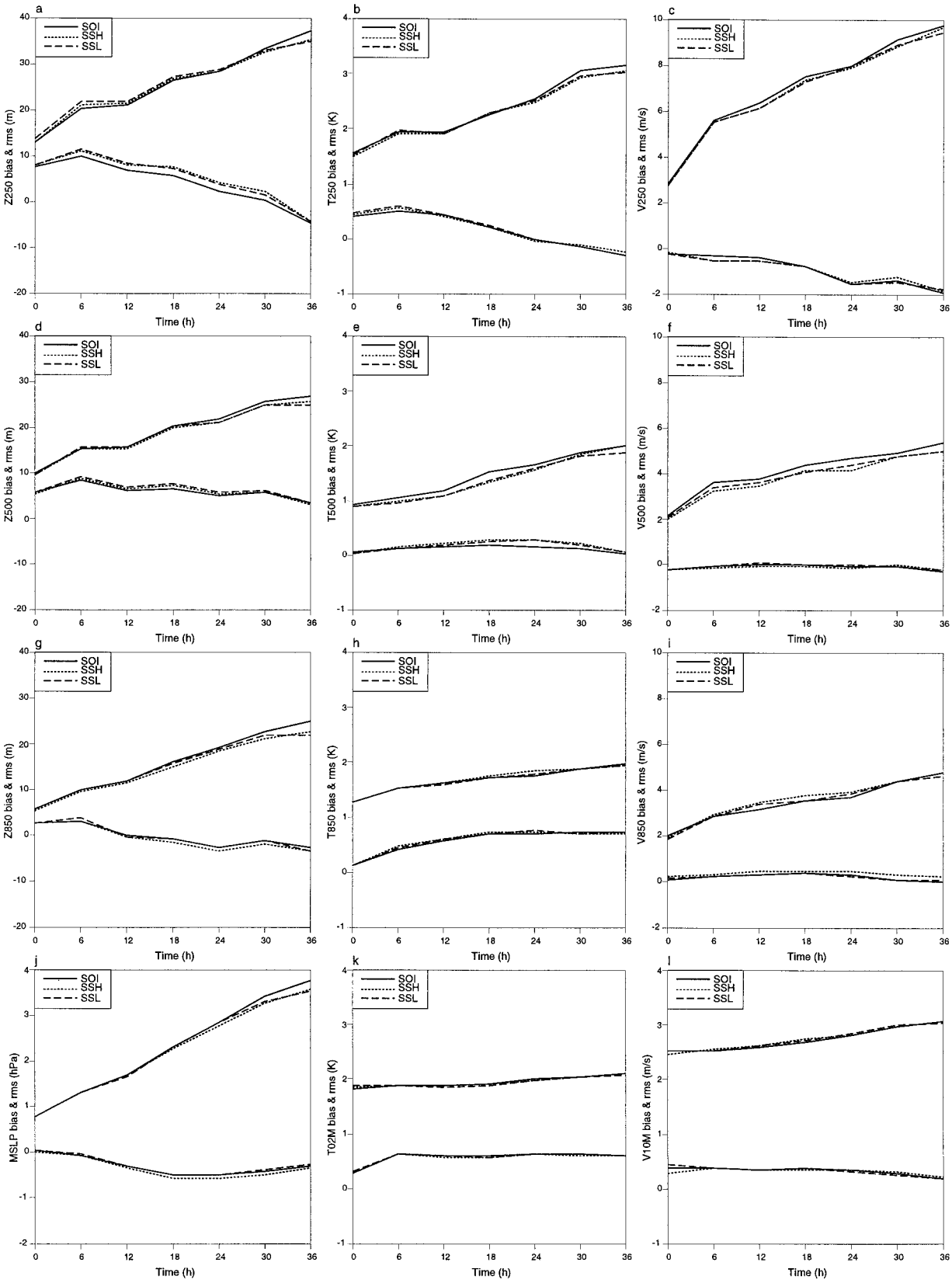

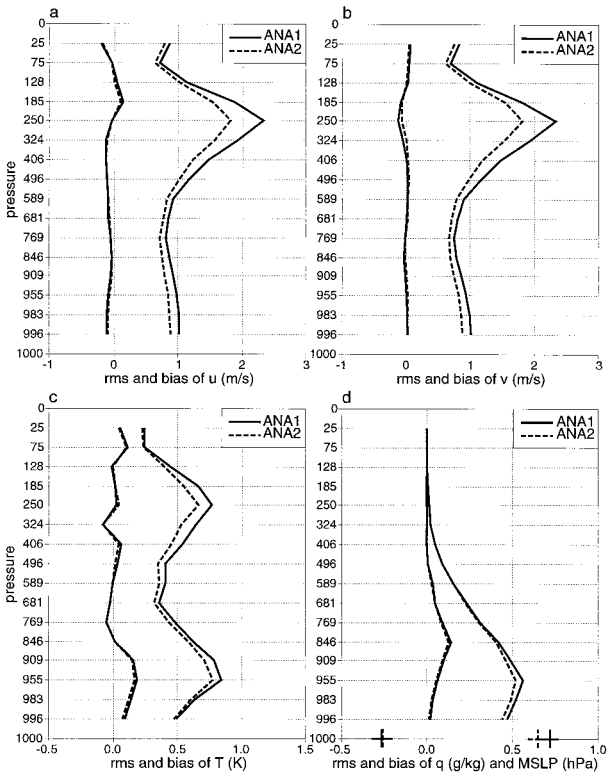

FIG. 9. Analysis increments, bias (left two curves in each panel), and rms (right two curves in each panel), in experiment SSH for horizontal winds u (a), v (b), temperature T (c), specific humidity q (d), and MSLP (bottom of d), averaged over the 5-day period (0000 UTC 13 Sep 1994–0000 UTC 18 Sep 1994). The full lines are for the preliminary analysis increments (ANA1). The dashed lines are for the final analysis (ANA2).

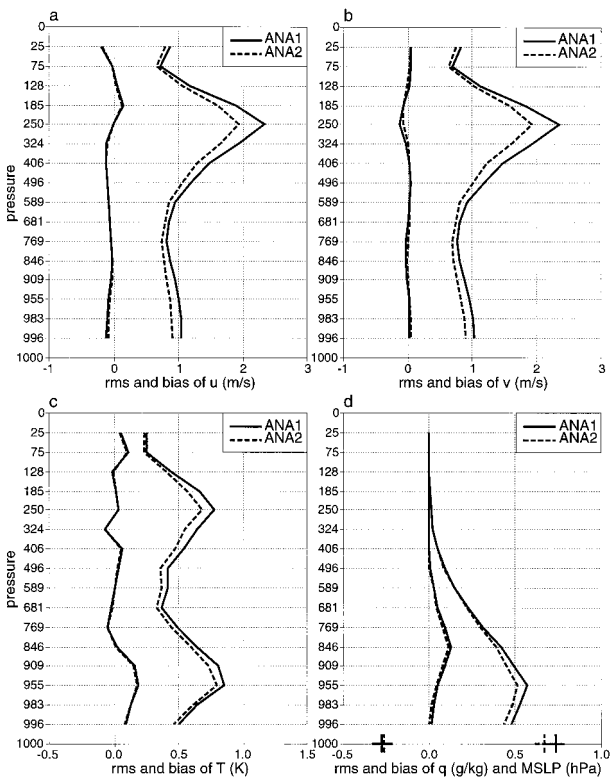

FIG. 10. Analysis increments, bias (left two curves in each panel), and rms (right two curves in each panel) in experiment SSL for horizontal winds u (a), v (b), temperature T (c), specific humidity q (d), and MSLP (bottom of d), averaged over the 5-day period (0000 UTC 13 Sep 1994–0000 UTC 18 Sep 1994). The full lines are for the preliminary analysis increments (ANA1). The dashed lines are for the final analysis (ANA2).

13. The largest differences appear over the ocean and are related to the jet stream. The differences increase with height. It is difficult to judge which analysis is better.

Because it is not obvious how to choose the verifying analyses, the field verification package has been run twice with GOI analyses and then with GSL analyses as references. Results of field verification against GOI analyses are given in Table 2. The upper part is for bias and the lower part is for rms. Forecasts at +12 h, +24 h, and +36 h from GOI and GSL experiments are compared directly with the GOI verifying analyses. When a GSL forecast is better than the corresponding GOI forecast, it is indicated by a star. Using GOI analyses as a reference, the verification results may be favorable for GOI. The overall impression is that GSL is better in bias and GOI is better in rms. However, at the end of forecasts (+36 h) GSL forecasts are better in mean sea level pressure, geopotential height, and wind at all levels. Results of field verification against GSL analyses are given in Table 3. From this table, it is evident that GSL forecasts are better than GOI forecasts in almost all selected parameters throughout the forecast range.

Finally, it is interesting to see the reduction in the analysis increments by GPV in GSL (Fig. 14). Although the variational first guess increment $F_2 - F_1$ is produced by a different forecast model and on a different resolution, the modifications to the preliminary first guess are in the right direction. The analysis increments in the final analysis are reduced for all model variables and at all model levels. The modified first guess fields are

←

FIG. 8. Observation verifications, bias (lower group of curves in each panel), and rms (upper group of curves in each panel) as functions of forecast length for SOI (full lines), SSH (dashed lines), and PMV (dotted lines) over the 5-day period (13–18 Sep 1994). (a) 250-Pa height, (d) 500-hPa height, (g) 850-hPa height, (b) 250-hPa temperature, (e) 500-hPa temperature, (h) 850-hPa temperature, (c) 250-hPa wind, (f) 500-hPa wind, (i) 850-hPa wind, (j) MSLP, (k), 2-m temperature, (l) 10-m wind.

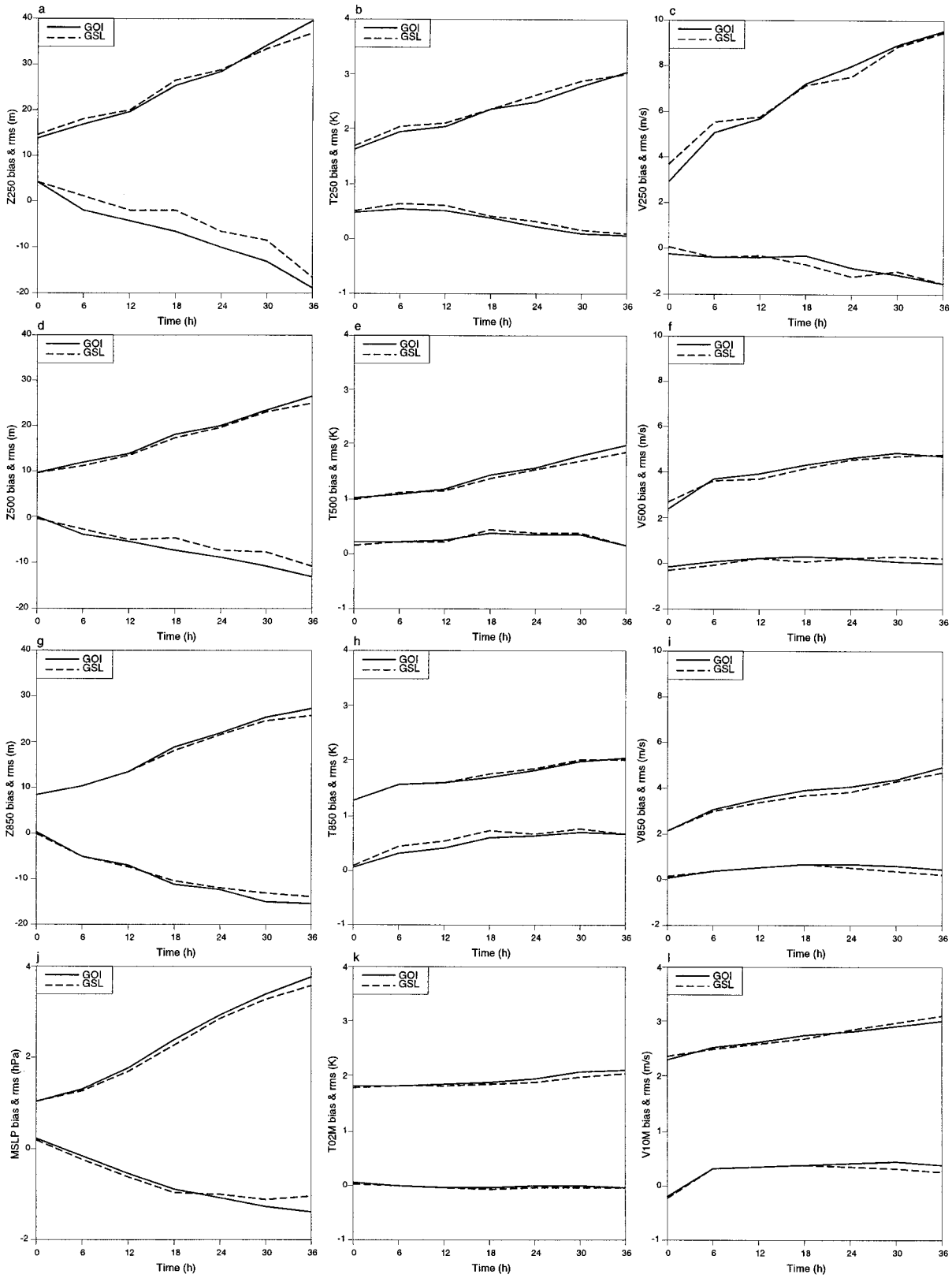

FIG. 11. Observation verifications, bias (lower group of curves in each panel), and rms (upper group of curves in each panel) as functions of forecast length for OIA (full lines) and PMV (dashed lines) over the 5-day period (13–18 Sep 1994). (a) 250-hPa height, (d) 500-hPa height, (g) 850-hPa height, (b) 250-hPa temperature, (e) 500-hPa temperature, (h) 850-hPa temperature, (c) 250-hPa wind, (f) 500-hPa wind, (i) 850-hPa wind, (j) MSLP, (k) 2-m temperature, (l) 10-m wind.

TABLE 2. Field verification against GOI analyses. An asterisk indicates GSL forecast is better than GOI forecast.

Variable		12 h		24 h		36 h	
		GOI	GSL	GOI	GSL	GOI	GSL
Z	250 bias	−21.69	−17.35	−29.35	−23.32*	−38.69	−31.44*
	500 bias	−4.13	−1.94*	−5.13	−1.82*	−4.35	−0.39*
	850 bias	−1.97	−0.23*	−8.80	−6.27*	−10.88	−6.43*
T	250 bias	0.00	0.06	−0.11	0.05*	−0.28	−0.24*
	500 bias	−0.06	−0.11	−0.02	−0.06	−0.01	−0.05
	850 bias	−0.11	−0.08*	−0.10	−0.07*	−0.05	−0.03*
	02m bias	−0.06	−0.07	−0.13	−0.13*	−0.16	−0.15*
V	250 bias	0.23	0.19*	0.19	0.19*	0.15	0.14*
	500 bias	0.10	0.09*	0.14	0.14*	0.13	0.13
	850 bias	0.07	0.08	0.13	0.13*	0.14	0.14*
	10m bias	0.06	0.06*	0.12	0.10*	0.14	0.12*
P	msl bias	0.12	0.13	0.09	0.10	0.06	0.10
Z	250 rms	135.80	143.59	212.48	214.85	285.96	281.38*
	500 rms	89.42	91.92	136.05	135.74*	182.09	179.48*
	850 rms	78.69	82.03	121.37	119.46*	159.93	155.62*
T	250 rms	1.14	1.29	1.63	1.69	2.00	2.03
	500 rms	0.64	0.79	1.02	1.08	1.37	1.39
	850 rms	0.97	1.07	1.26	1.29	1.51	1.52
	02m rms	0.58	0.70	0.90	0.92	1.12	1.13
V	250 rms	5.32	6.14	7.77	7.99	9.36	9.32*
	500 rms	2.72	3.43	4.40	4.57	5.63	5.60*
	850 rms	2.13	2.42	3.37	3.37*	4.31	4.29*
	10m rms	1.72	1.89	2.46	2.50	3.03	3.04
P	msl rms	1.19	1.26	1.77	1.75*	2.27	2.23*

therefore closer to observations than the preliminary ones.

To summarize the results in this section, the following points may be stated.

- The low-resolution variational component based on the spectral HIRLAM model and its adjoint (in experiment GSL) can be used together with the data assimilation system based on the gridpoint HIRLAM model. In general, GSL gives better forecast scores than GOI. The reduction in analysis increments by GSL looks similar to that in the previous section. This answers the second question raised in the introduction; that is, the variational component in the GPV data assimilation system can be based on a different model formulation, which gives rise to the flexibility of an operational implementation.
- Although not being explicitly discussed, there is no obvious problem related to using ECMWF forecasts as lateral boundary conditions. A preoperational test with GSL setup has no technical difficulty.
- The differences between the original OI analyses and the GPV analyses are mainly over the ocean where observations are sparse. The amplitude and horizontal scale of the differences increase with height. A clear correlation between the difference pattern and the basic flow indicate that GPV analyses have modified baroclinic structures. These structures seem to be beneficial as the GSL forecasts are generally better than the GOI forecasts.

6. Conclusions

In this paper, a generalized scheme (GPV) is proposed for the poor man's four-dimensional variational data assimilation system (PMV) of Huang et al. (1997). The basic idea of the generalized scheme is the same as that of the original, that is, to use the adjoint model to improve the first guess in intermittent data assimilation systems. The main advantage of the generalized scheme is its implementation flexibility, which allows the use of an independently developed adjoint model in OI/3DVAR-based data assimilation systems and leads to CPU and disk storage savings.

A detailed comparison is made between the generalized scheme and the original one. The steps of a practical implementation are also given. The variational component of the generalized scheme is completely incremental. The extra CPU cost is about two 6-h non-

→

FIG. 12. Geopotential height analyses averaged over the 5-day period for (a) GOI at 250 hPa, (b) GSL at 250 hPa, (c) GOI at 500 hPa, (d) GSL at 500 hPa, (e) GOI at 850 hPa, and (f) GSL at 850 hPa. The contour interval is 4 dm.

FIG. 13. Differences between GSL and GOI geopotential height analyses for (a) bias at 250 hPa, (b) standard deviation (std) at 250 hPa, (c) bias at 500 hPa, (d) std at 500 hPa, (e) bias at 850 hPa, (f) std at 850 hPa. The contour interval is 2 m. Full line is positive. Dashed line is negative. Zero line is suppressed. Within the shaded area, std $>$ 6 m.

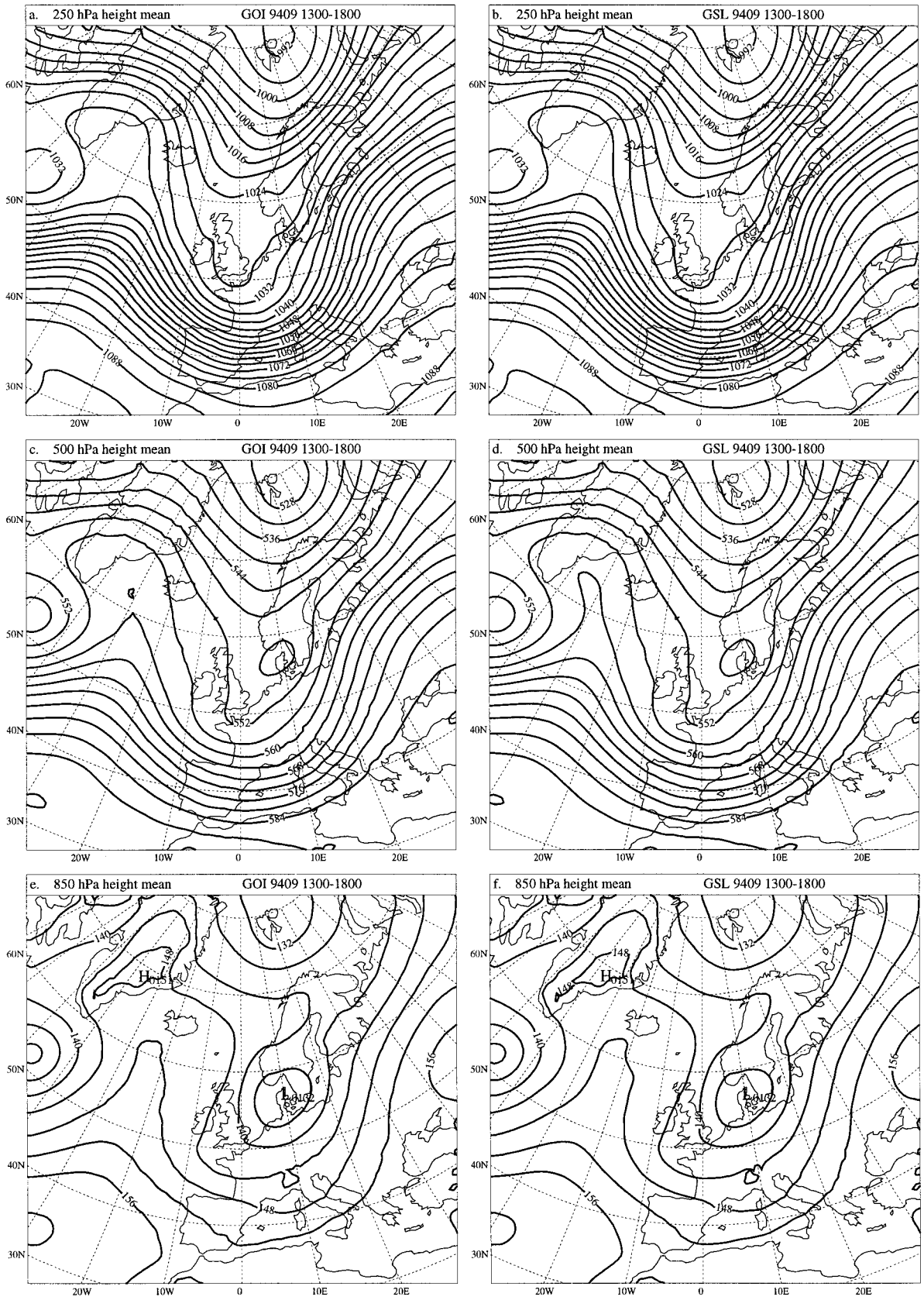

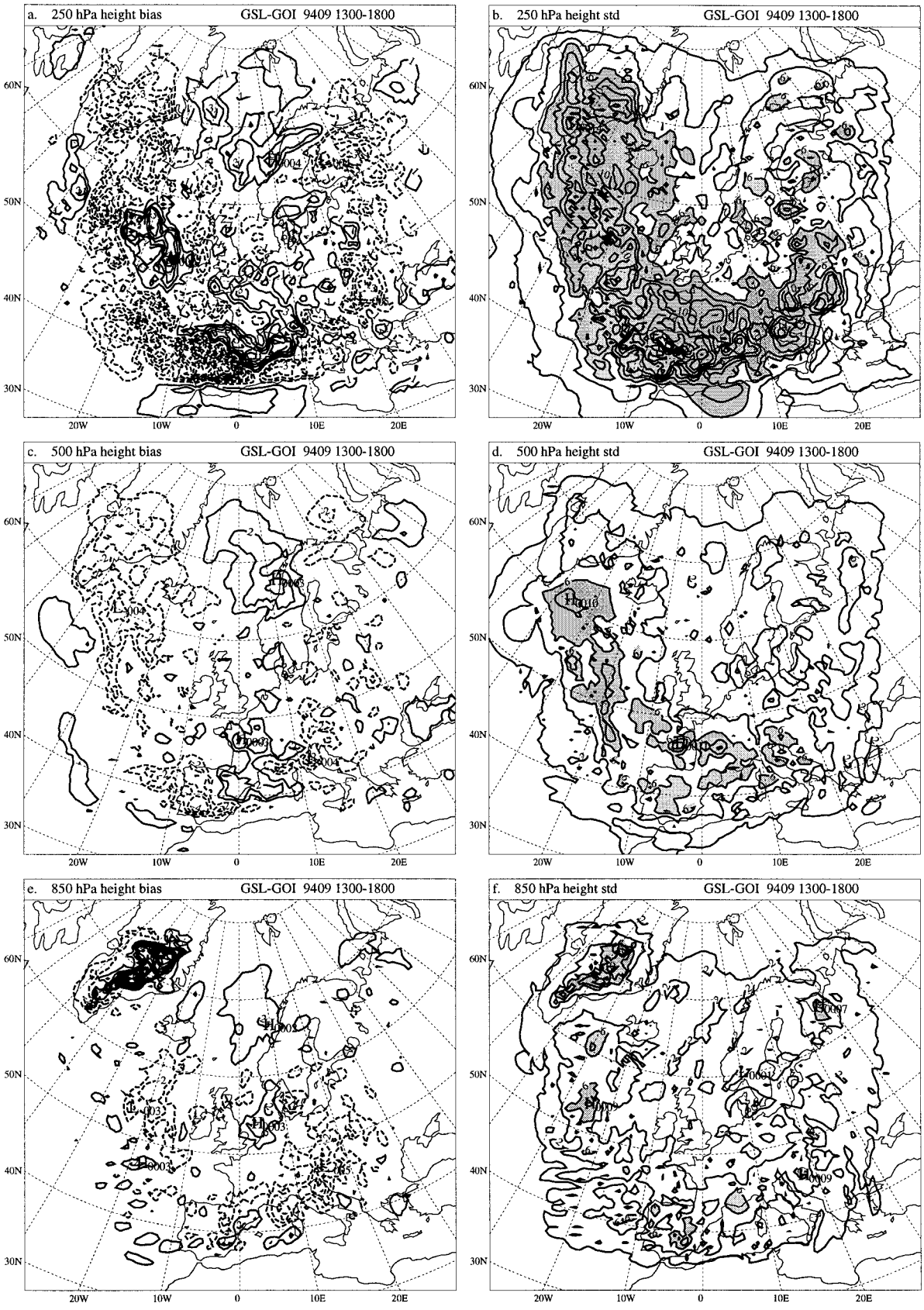

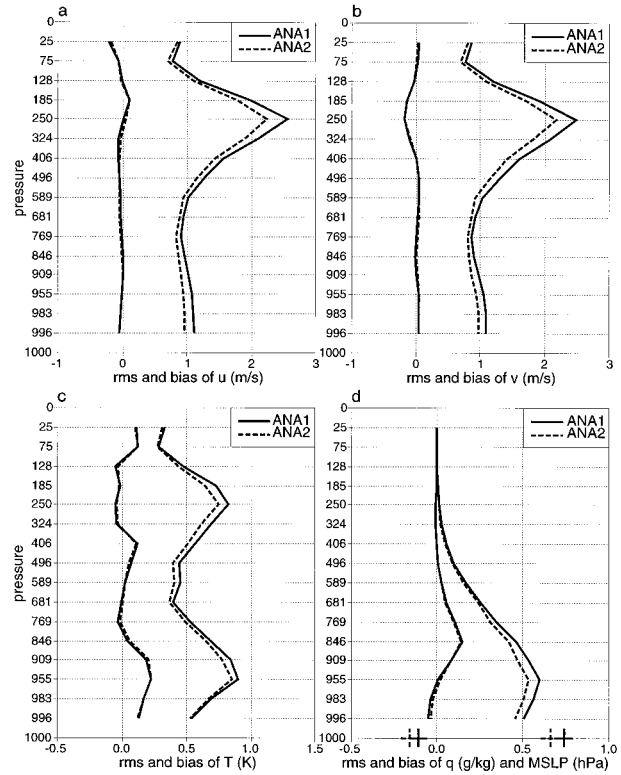

FIG. 14. Analysis increments, bias (left two curves in each panel), and rms (right two curves in each panel) in experiment GSL for horizontal winds u (a), v (b), temperature T (c), specific humidity q (d), and MSLP (bottom of d), averaged over the 5-day period (0000 UTC 13 Sep 1994–0000 UTC 18 Sep 1994). The full lines are for the preliminary analysis increments (ANA1). The dashed lines are for the final analysis (ANA2).

linear runs plus one 6-h adjoint run. With a low-resolution variational component, the extra cost is reduced; for example, with the resolution of two-thirds of the original, the extra cost of GPV is about a 6-h forecast plus the final analysis.

It is shown in this paper that the generalized scheme works as expected. Running the variational component on low resolutions and with a different model formulation does not alter the the conclusion of Huang et al. (1997): the use of an adjoint model in intermittent data assimilation systems leads to better first guess fields, smaller analysis increments, modified baroclinic structures in the final analyses and improved forecasts.

The differences between the original OI-based analyses and the adjoint model modified analyses are mainly in the data sparse area and are related to baroclinic processes. The 5-day average of the analysis differences has large values over the Atlantic and along the mean trough. The difference increases with height. Although it is difficult to evaluate the two analysis sets directly using the very limited number of observations, the analyses modified by the adjoint model seem to be better than the original OI-based analyses judging from the 21 forecasts on the 5-day average.

With an operational implementation in mind, we have also removed the idealized assumption on lateral bound-

TABLE 3. Field verification against GSL analyses. An asterisk indicates GSL forecast is better than GOI forecast.

	Variable	12 h		24 h		36 h	
		GOI	GSL	GOI	GSL	GOI	GSL
Z	250 bias	−20.76	−16.42*	−28.96	−22.93*	−38.54	−31.29*
	500 bias	−4.20	−2.01*	−5.65	−2.34*	−5.58	−1.62*
	850 bias	−2.71	−0.97*	−10.05	−7.52*	−12.51	−8.07*
T	250 bias	−0.08	−0.02*	−0.18	−0.13*	−0.34	−0.30*
	500 bias	−0.01	−0.06	0.04	0.00*	0.05	0.01*
	850 bias	−0.12	−0.09*	−0.11	−0.07*	−0.05	−0.03*
	02m bias	−0.02	−0.03	−0.09	−0.09*	−0.13	−0.12*
V	250 bias	0.22	0.18*	0.19	0.19*	0.15	0.13*
	500 bias	0.07	0.06*	0.11	0.11*	0.12	0.12*
	850 bias	0.08	0.09	0.14	0.13*	0.15	0.15*
	10m bias	0.08	0.08*	0.14	0.13*	0.15	0.14*
P	msl bias	0.11	0.12	0.07	0.09	0.04	0.08
Z	250 rms	146.82	145.97*	215.07	215.93	285.08	279.60*
	500 rms	95.95	93.91*	139.20	137.65*	185.17	182.30*
	850 rms	83.74	82.01*	124.10	121.49*	162.71	158.32*
T	250 rms	1.41	1.31*	1.78	1.78	2.08	2.11
	500 rms	0.83	0.77*	1.12	1.12	1.43	1.41*
	850 rms	1.09	1.01*	1.33	1.30*	1.55	1.54*
	02m rms	0.78	0.65*	1.01	0.97*	1.19	1.19*
V	250 rms	9.06	8.78*	10.05	10.09	10.96	10.94*
	500 rms	4.70	4.29*	5.65	5.59*	6.49	6.42*
	850 rms	3.12	2.88*	3.97	3.86*	4.66	4.61*
	10m rms	2.12	1.95*	2.72	2.68*	3.19	3.19*
P	msl rms	1.27	1.23*	1.80	1.77*	2.30	2.25*

ary conditions. Instead of using future analyses, which is impossible for operational conditions, ECMWF forecasts available at the analysis time are used in the last two experiments. From observation verification and field verification, there seems to be no obvious problem related to boundaries. This may be case dependent. As recently shown by Zou et al. (1995), Zou and Kuo (1996), and Gustafsson et al. (1998), it is important under certain weather situations to control the lateral boundaries. In such situations, the adjoint model run should have lateral boundary included as a control variable.

Only a 5-day period is studied in this paper. The weather situation of the period was dominated by an intense cyclone. All verification results may just be a reflection of the improvements for this cyclone forecast. At the time of the writing, preoperational tests of the generalized scheme are planned for two weeks in winter and two weeks in summer. These tests will be reported separately.

Acknowledgments. The author would like to thank Nils Gustafsson, Erland Källén, Peter Lynch, and Xiaohua Yang for many discussions during this work and comments on an earlier version of the manuscript. Thanks are also given to Bjarne Amstrup for his assistance in running the DMI observation and field verification packages; Jess Jørgensen for his assistance in running the DMI operational data assimilation system; Leif Laursen for his continued support; and anonymous reviewers for their comments.

APPENDIX A

GPV in a Formula Form

Using a^n and a^{n+1} to indicate analyses at previous cycle and at current cycle, respectively, a formula of the GPV can be written as

$$a^{n+1} = A\{\underbrace{Ma^n}_{\text{pre fgs}} + \underbrace{RG^cS^uV[RS^dG^aa^n + \alpha L^T(\overbrace{RS^dG^aAMa^n}^{\text{pre ana}} - \overbrace{VRS^dG^aa^n}^{\text{aux fcst}})]}_{\text{sen fcst}} - \underbrace{RG^cS^uVRS^dG^aa^n}_{\text{aux fcst}}\}, \quad \text{modified firstguess}$$

(adjoint model run)

where we see the following (in the following list, the actual scheme used in this study is given in the parentheses).

- A The OI or 3DVAR analysis. (The HIRLAM OI scheme.)
- M The original forecast model. (The spectral HIRLAM model in section 4 and the gridpoint HIRLAM model in section 5.)
- V The forecast model used in the adjoint model development. (The spectral HIRLAM model.)
- L^T The adjoint of V. (The adjoint of the spectral HIRLAM.)
- α The optimal step size used in minimization.
- G^a Grid transform (from C grid to A grid).
- G^c Grid transform (from A grid to C grid).
- S^d From the original resolution to low resolution. (Remove high wavenumber components.)
- S^u From low resolution to the original resolution. (Fill the additional high wavenumber components with zeros.)
- R The adjustment to the corresponding orography.

When M and V are the same and the same resolution is used, that is, replace V by M and ignore R, G^a, G^c, S^d, and S^u, the above GPV formula is reduced to the one for PMV as

$$a^{n+1} = A\{\underbrace{M[a^n + \alpha L^T(\overbrace{AMa^n}^{\text{pre ana}} - \overbrace{Ma^n}^{\text{pre fgs}})]}_{\text{sen fcst = modified firstguess}}\}.$$

(adjoint model run)

The original OI scheme can be obtained by setting α to zero; that is, no modification is made to the preliminary first guess:

$$a^{n+1} = AMa^n.$$

APPENDIX B

The HIRLAM Analysis

The HIRLAM analysis is a limited-area version of the ECMWF OI scheme (Lönnberg and Shaw 1987; Haseler 1988). The adaption to the limited area has been documented in a HIRLAM technical note (Gustafsson and Järvenoja 1987) and the latest HIRLAM manual (Källén 1996). A brief description of the scheme is given here.

The scheme is based on the optimum interpolation (Eliassen 1954; Gandin 1963) extended to multivariate three-dimensional interpolation of observed deviations from forecast first guess fields (Lorenc 1981). Analysis

parameters are geopotential, wind components, and relative humidity. Analysis increments are evaluated on the forecast model levels on a nonstaggered grid (A grid).

Geopotential and wind components are analyzed simultaneously with an assumption of near-linear geostrophic balance between the rotational part of the wind analysis increment and the geopotential analysis increment. The incremental streamfunctions and geopotentials are assumed to be correlated with a factor 0 at the equator and 0.95 north of 30°N with a gradual transition in the zone between the equator and 30°N. Relative humidity is analyzed univariately.

Three-dimensional correlations of true minus first guess are modeled by assuming them to be products of horizontal and vertical correlations. The vertical correlations are modeled by fitting analytic functions to empirically determined vertical correlations. Isotropic correlation models for geopotential, streamfunction, velocity potential, and relative humidity are used in the horizontal. Series of zero-order Bessel functions, fitted to empirical correlations from time series of historical ECMWF forecast errors (Hollingsworth and Lönnberg 1986; Lönnberg and Hollingsworth 1986) are used to represent these isotropic horizontal correlations. The series of zero-order Bessel functions include nine terms in order to represent also smaller-scale features of interest for high-resolution analysis. As regards the variance of the wind fields first guess error, 90% of the variance is assumed to be nondivergent and 10% is assumed to be divergent. Generally, the variance of forecast first guess error is obtained from the estimated variance of the analysis errors of the previous analysis cycle by assuming a linear growth in time toward the climate error variance over a specified time period. This time period has been set to 96 h in HIRLAM, whereas ECMWF used a corresponding time period of 144 h. This increase of assumed error growth rate will result in increased assumed variance of first guess errors and consequently in a closer fit of the analysis fields to the observations for the HIRLAM analysis scheme compared to the ECMWF OI implementation.

In the analysis, the three-dimensional model domain is divided into boxes. In each box, the same observations influence all grid points. As a consequence, multivariate relationships are more efficiently used. To analyze horizontal scales larger than the horizontal box size and to have a smoother transition in the analysis fields from box to box, observations outside the analysis box are also selected to influence the analysis of grid points in the box. In addition, a further averaging between neighboring boxes is performed to smooth out possible discrepancies between analysis values near the box boundaries. The largest horizontal box size in HIRLAM OI is 330 km with a limit distance of influencing observations of 930 km away from the center of the analysis box.

The observation window covers a 6-h span around the analysis times (0000, 0600, 1200, and 1800 UTC). A standard observation set is used, including synoptic observations (SYNOP), ship observations (SHIP), drifting buoys (DRIBU), pilot balloons (PILOT), radiosondes (TEMP), and aircraft data (AIREP). TEMP geopotential and wind data close to 15 predetermined pressure levels, and TEMP humidity data close to five predetermined pressure levels (only within troposphere) are used. PILOT wind observations are treated in the same way as TEMP winds. Observed sea level pressure or station level pressure from SYNOP, SHIP, and DRIBU reports as well as single-level wind reports from SHIP and AIREP reports are utilized at the reporting levels. Each observation is associated with an estimated standard deviation of observational error. TEMP data is assumed to have vertically correlated observational errors and a model for this correlation is used. No horizontal correlation is assumed for observational errors.

The HIRLAM OI scheme has a comprehensive quality control of all observations. The quality control includes a check against forecast first guess values; a check for multilevel vertical consistency; and a check against an analysis that is derived without the observation in concern. It also ''blacklists'' observations from stations or platforms, which, in the data monitoring, have been found to be systematically in error or contaminated by frequent large random errors.

The analysis is carried out in the following sequence: 1) extraction of observations; 2) interpolate first guess fields and first guess error standard deviations to the observation positions; 3) formation of ''super observations'' by averaging observations of the same type over areas corresponding to the analysis grid resolution; 4) analysis check and final acceptance of observations; 5) computation of an analysis vector for each analysis box; 6) evaluation of analysis increments for all forecast model grid points.

REFERENCES

Arakawa, A., and V. R. Lamb, 1977: Computational design of the basic dynamical processes of the UCLA general circulation model. *Methods Comput. Phys.,* **17,** 174–265.

Courtier, P., J. N. Thépaut, and A. Hollingsworth, 1994: A strategy for operational implementation of 4D-Var, using an incremental approach. *Quart. J. Roy. Meteor. Soc.,* **120,** 1367–1387.

Derber, J. C., 1987: Variational four-dimensional analysis using quasi-geostrophic constraints. *Mon. Wea. Rev.,* **115,** 998–1008.

——, D. F. Parrish, and S. J. Lord, 1991: The new global operational analysis system at the National Meteorological Center. *Wea. Forecasting,* **6,** 538–547.

Eliassen, A., 1954: Provisional report on calculation of spatial covariance and autocorrelation of the pressure field. Rep. 5, Norwegian Academy of Sciences, Institute of Weather and Climate Research, Oslo, Norway, 12 pp.

Gandin, L., 1963: *Objective Analysis of Meteorological Fields* (in Russian). Gidromet.

Gustafsson, N., 1991: The HIRLAM model. *Proc. ECMWF Sem. on Numerical Methods in Atmospheric Models,* Vol. 2, Reading, United Kingdom, ECMWF, 115–146.

——, Ed., 1993: HIRLAM 2 final report. HIRLAM Tech. Rep. 9, 126 pp. [Available from SMHI, S-601 76 Norrköping, Sweden.]

——, and S. Järvenoja, 1987: Sensitivity tests with a limited area version of the ECMWF analysis scheme. HIRLAM Tech. Note 3. [Available from DMI, DK-2100 Copenhagen, Denmark.]
——, and X.-Y. Huang, 1996: Sensitivity experiments with the spectral HIRLAM and its adjoint. *Tellus,* **48A,** 501–517.
——, E. Källén, and S. Thorsteinsson, 1998: Sensitivity of forecast errors to initial and lateral boundary conditions. *Tellus,* **50A,** 167–185.
Haseler, J., Ed., 1988: ECMWF data assimilation—Program documentation. ECMWF Res. Man. 5. [Available from ECMWF, Shinfield Park, Reading, Berkshire RG2 9AX, United Kingdom.]
Hollingsworth, A., and P. Lönnberg, 1986: The statistical structure of short-range forecast errors as determined from radiosonde data. Part I: The wind field. *Tellus,* **38A,** 111–136.
Huang, X.-Y., A. Cederskov, and E. Källén, 1994: A comparison between digital filtering initialization and nonlinear normal mode initialization in a data assimilation system. *Mon. Wea. Rev.,* **122,** 1001–1015.
——, N. Gustafsson, and E. Källén, 1997: Using an adjoint model to improve an optimum interpolation-based data assimilation system. *Tellus,* **49A,** 161–176.
Källén, E., Ed., 1996: HIRLAM documentation manual. System 2.5. [Available from SMHI, S-601 76 Norrköping, Sweden.]
Le Dimet, F., and O. Talagrand, 1986: Variational algorithms for analysis and assimilation of meteorological observations: Theoretical aspects. *Tellus,* **38A,** 97–110.
Lewis, J., and J. Derber, 1985: The use of adjoint equations to solve a variational adjustment problem with advective constraints. *Tellus,* **37A,** 309–327.
Lönnberg, P., and A. Hollingsworth, 1986: The statistical structure of short-range forecast errors as determined from radiosonde data. Part II: The covariance of height and wind errors. *Tellus,* **38A,** 137–161.
——, and D. Shaw, Eds. 1987: ECMWF data assimilation—Scientific documentation. ECMWF Res. Man. 1. [Available from ECMWF, Shinfield Park, Reading, Berkshire RG2 9AX, United Kingdom.]
Lorenc, A. C., 1981: A global three-dimensional multivariate statistical interpolation scheme. *Mon. Wea. Rev.,* **109,** 701–721.
Machenhauer, B., Ed., 1988: HIRLAM final report. HIRLAM Tech. Rep. 9, 116 pp. [Available from DMI, DK-2100 Copenhagen Ø, Denmark.]
Navon, I. M., X. Zou, J. Derber, and J. Sela, 1992: Variational data assimilation with an adiabatic version of the NMC spectral model. *Mon. Wea. Rev.,* **120,** 1433–1446.
Parrish, D. F., and J. C. Derber, 1992: The National Meteorological Center's Global spectral statistical interpolation analysis system. *Mon. Wea. Rev.,* **120,** 1747–1763.
Pu, Z.-X., E. Kalnay, and J. G. Sela, 1997a: Sensitivity forecast errors to initial conditions with a quasi-inverse linear method. *Mon. Wea. Rev.,* **125,** 2479–2503.
——, ——, J. C. Derber, and J. G. Sela, 1997b: Using forecast sensitivity patterns to improve future forecast skill. *Quart. J. Roy. Meteor. Soc.,* **123,** 1035–1054.
Rabier, F., E. Klinker, P. Courtier, and A. Hollingsworth, 1996: Sensitivity of two-day forecast errors over the Northern Hemisphere to initial conditions. *Quart. J. Roy. Meteor. Soc.,* **122,** 121–150.
Thépaut, J.-N., and P. Courtier, 1991: Four-dimensional variational data assimilation using the adjoint of a multilevel primitive-equation model. *Quart. J. Roy. Meteor. Soc.,* **117,** 1225–1254.
——, D. Vasiljević, P. Courtier, and J. Pailleux, 1993: Variational assimilation of conventional meteorological observations with a multilevel primitive equation model. *Quart. J. Roy. Meteor. Soc.,* **119,** 153–186.
Wang, Z., K. K. Droengemeier, L. White, and I. M. Navon, 1997: Application of a new adjoint Newton algorithm to the 3D ARPS storm-scale model using simulated data. *Mon. Wea. Rev.,* **125,** 2460–2478.
Yang, W., I. M. Navon, and P. Courtier, 1996: A new Hessian preconditioning method applied to variational data assimilation experiments using NASA general circulation models. *Mon. Wea. Rev.,* **124,** 1000–1017.
Zou, J., W. W. Hsieh, and I. M. Navon, 1995: Sequential open-boundary control by data assimilation in a limited-area model. *Mon. Wea. Rev.,* **123,** 2899–2909.
Zou, X., and Y.-H. Kuo, 1996: Rainfall assimilation through an optimal control of initial and boundary conditions in a limited-area mesoscale model. *Mon. Wea. Rev.,* **124,** 2859–2882.
Županski, M., 1993: Regional four-dimensional variational data assimilation in a quasi-operational forecasting environment. *Mon. Wea. Rev.,* **121,** 2396–2408.
——, 1996: A preconditioning algorithm for four-dimensional variational data assimilation. *Mon. Wea. Rev.,* **124,** 2562–2573.